Research Journal of Chemical Sciences _____ISSN 2231-606X
Vol. **7(4),** 24-33, April **(2017)** *Res. J. Chem. Sci.*

Preparation of magnetic iron oxide nanoparticles activated carbon composite from corncob and its application for removal of organic pollutants

Shripal Singh* and Rinku Jaiswal
CIMFR Nagpur Unit-II, 17/C-Telenkhedi area, Civil Lines, Nagpur-440001, India
shripal_singh@yahoo.co.uk

Available online at: www.isca.in, www.isca.me
Received 14th January 2017, revised 11th March 2017, accepted 14th April 2017

Abstract

Magnetic iron oxide nanoparticles are attractive to many researchers because of their wide ranging applications viz. data storage, magnetic fluids, adsorbent, catalysis, biotechnology, biomedicine and environmental remediation. In the present study, efforts have been made to develop magnetic iron oxide nanoparticles activated carbon composite (MIONAC). The activated carbon is prepared from corncob using zinc chloride as an activating agent in a modified muffle furnace with N_2-gas inflow arrangement and magnetic nanoparticles by chemical co-precipitation method. The prepared corncob activated carbon (CCAC) and Magnetic iron oxide nanoparticles activated carbon composite (MIONAC) are characterized for N_2-BET surface area, SEM, FT-IR, XRD, TEM, pHpzc and VSM. The N_2-BET surface area of the MIONAC (807 m^2g^{-1}) is found lesser than the prepared CCAC (1429 m^2g^{-1}). MIONAC exhibits super magnetic properties under external magnetic field with saturation magnetization value 4.15 emu/g at room temperature. SEM of the CCAC and MIONAC shows the presence of cracks and crevices. TEM of MIONAC shows nanoparticles with size in between 10-20 nm. A broad peak at $2\theta = 24^0$ in XRD of CCAC and MIONAC indicates the presence of amorphous carbon. The adsorption isotherms and kinetic studies using CCAC and MIONAC as adsorbents and phenols as adsorbates. The adsorption data shows that the adsorption capacity (Q_0) value of MIONAC (90 mg/g) is slightly lesser than the CCAC (125 mg/g). Langmuir kinetic model best suits for determination of adsorption and desorption constants for organic pollutants phenols on both CCAC & MIONAC.

Keywords: Corncob, Chemical coprecipitation, Magnetic nanoparticles, Phenols, Adsorption isotherm, Kinetics.

Introduction

Many industrial wastes contain organics which are hazardous and non-biodegradable. Phenols as a class of organic compounds are toxic in nature and slightly pungent and bad in odour. Removal of these pollutants from wastewater has become great challenge to wastewater treatment technologies. Various treatment technologies viz. steam distillation, oxidation using strong oxidising agent, coagulation, filtration, reverse osmosis, photo catalytic treatment and adsorption on activated carbon have been developed to minimize organic pollutants. However, adsorption onto surface of activated carbon has been proved one of the most efficient and economically viable methods for removal of these priority organic pollutants, namely phenol, o-cresol, p-nitrophenol and aniline. There are several reports on adsorption of organic pollutants on activated carbon. Casta and Rodrigues studied the adsorption of phenol and p-nitrophenol from aqueous phase on GAC[1] and interpreted experimental data by IAS theory formulated by Radke and Prausnitz[2]. Chern and Chien investigated competitive adsorption of benzoic acid and p- nitrophenol onto activated carbon and concluded that GAC has higher affinity to PNP than Benzoic acid[3]. Fritz and Schlunder proposed a general empirical equation for calculating the adsorption equillibria of organic solutes in solution and successfully tested for aqueous solution of phenol and p-nitrophenol[4]. Srivastava and Tyagi Studied competitive of substituted phenols by activated carbon developed fertilizer waste slurry[5]. Khan et al presented adsorption of phenol-based organic pollutants on activated carbon from multi-component dilute aqueous solutions[6].

Activated carbon, a widely used adsorbent, is mainly composed of carbonaceous material with high surface area and porous structure[7]. The extensive application of activated carbon is mainly due to its high adsorption capacity and cheap or zero cost of the starting carbonaceous materials used for the preparation. Numerous studies have been devoted to preparation of low-cost high quality carbon adsorbents for treatment and purification of water, air as well as various chemical and natural products[8]. The raw materials being used are usually carbonaceous materials like wood[9], coal[10], nut shells[11], husks[12] and most agricultural by-products materials[13]. Typically agricultural by-products or wastes such as olive cake[14], bagasse[15], coconut husk1[6], and palmshell[17] are used as the starting materials to prepare activated carbon.

Nowadays, nanoparticles are not only widely applied in the fields of medicine, molecular biology and bioinorganic chemistry, but they are also well known in environmental science[18]. The main advantage of this technology consists in its capacity of treating large amount of wastewater within a short time and producing less contamination[19]. Magnetic filtration is

emerging as a water treatment technology, which can provide rapid, efficient contaminant removal from aqueous waste streams[20]. MIONAC adsorbents can easily be separated from a solution using a magnetic retriever.

In this work Magnetic iron oxide nanoparticles activated carbon was prepared by coprecipitation method for the removal of phenol from aqueous solution.

Materials and methods

The corncobs were collected from the local market of Nagpur City (India), crushed and sieved through 5mm and 2mm sieves to get -5 to +1mm size fraction. The screened mass is washed with distilled water to remove any dirt and dried. All chemicals used were analytical grade obtained from Merck, India.

Preparation of activated carbon: The -5 to +1mm sized corncobs were impregnated with zinc chloride in different ratios and kept undisturbed for 24 hours. Impregnated material was carbonized in a modified muffle furnace with N_2 gas inflow arrangement at 500-900 ^{0}C for 1-3 hours. After carbonization, the sample was de-ashed with 5N HCl followed by washing with distilled water. The washed carbon was dried at 108±2^{0}C in a moisture oven for 24 hours and kept in a desiccator.

Preparation of magnetic iron oxide nanoparticles activated carbon composite (MIONAC): The Magnetic iron oxide nanoparticles activated carbon composite (MIONAC) was made by a chemical co-precipitation method. Synthesis of iron oxide magnetic nanoparticles was carried out by co-precipitation method of ferric and ferrous salts under the presence of N_2 gas. 17g $FeCl_3$ and 7g of $FeCl_2$ were dissolved in 250 ml of deoxygenated distilled water. After stirring for 60 minutes, chemical precipitation was achieved at 35^{0}C under vigorous stirring by adding of 2M NaOH solution under the presence of N_2 gas. The reaction system was kept at 70^{0}C for 6 h and pH of solution 10-11. Complete precipitation of Fe_3O_4 expected at pH between 8 and 14 [21]. Later the system was cooled to room temperature and the precipitate was separated by a permanent magnet. This precipitate was washed with deoxygenated distilled water until pH of the washing was neutral. Finally Fe_3O_4 was washed with acetone and dried in an oven at 60-70^{0}C. The relevant chemical reaction can be shown as follows;

$$Fe^{2+} + 2Fe^{3+} + 8OH^- \rightarrow Fe_3O_4 + 4H_2O \quad (1)$$

To prepare MIONAC, Fe_3O_4 magnetic nanoparticles were combined with aqueous suspension of activated carbon. In the first step, a known quantity of activated carbon was impregnated with nitric acid (63%) and kept undisturbed for 3h at 100°C by using an ultrasonic bath. The sample was then filtered and dried in a room temperature. Subsequently, aqueous suspension of 5g obtained activated carbon was added into 200 ml of aqueous solution containing $Fe_3O_4.9H_2O$ and placed in ultrasonic bath for 1 h at 100°C. Then the sample was filtered and dehydrated in an oven at 100°C for 1 h. The sample was heated in a muffle furnace at 800°C for 3h under nitrogen gas atmosphere. The synthesized MIONAC was washed with deionised water for four times and then dried at a 100°C in a moisture oven and kept in a desiccator for use.

Method for adsorption isotherm and kinetics study: For adsorption isotherm and kinetics experiments, adsorbate solutions of different concentrations were prepared by diluting the stock solution with calculated volume of water. The initial concentration was analyzed by ultraviolet-visible spectrophotometer.

Adsorption kinetics was monitored by adding 3g weighed CCAC and MIONAC were introduced into 3L of phenol solution of known concentration with constant stirring at 30°C stirred at 180 rpm. The whole system was kept in a thermostatic water bath.

Characterization of raw material and prepared CCAC and MIONAC: Proximate and ultimate analysis: The proximate of CCAC and MIONAC were carried out as per IS 1350 (part 1), 1974 and ultimate analysis by CHNSO analyser microcube, Elementar, Germany. The quality of prepared activated carbon depends on the source material and method of preparation. Proximate analysis and ultimate analysis results of raw material, prepared CCAC and MIONAC are reported in Table-1 and 2. The proximate data of raw material shows low ash content; 5.8% and high volatile matter; 77%. The ultimate analysis (on dry mineral matter free basis) of raw material shows carbon of 60.93% and hydrogen 8.26%. It can be concluded from the proximate and ultimate data that the Corncobs are very suitable raw material for preparing activated carbon. The proximate and ultimate analysis of prepared CCAC shows very high moisture (26.7%), low ash (2.6%) and high carbon content (81.40%). In comparison, of CCAC, MIONAC shows high ash content (15.2%) and low carbon content (56.6%). This is due to dispersion of Fe_3O_4 nanoparticle in the CCAC pores.

Iodine number, N_2-BET Surface area and pore volume: To determine micro pores structure of CCAC and MIONAC, iodine number, surface area and pore volume as shown in Table-3. The iodine number and surface area reduces in MIONAC because, pores of CCAC with Fe_3O_4 nanoparticles.

Scanning electron microscopy: The surface morphology of CCAC and MIONAC were studied from SEM. The SEM micrographs of CCAC and MIONAC are shown in Figure-1 (a, b) and Figure-1 (c) respectively. A porous, spongy texture in the case of CCAC can be seen in Figure-1 (a, b). The micrograph, Figure-1(c) show the morphological changes due to iron oxide impregnation on the surface of the carbon matrix with mass ratio of 1/2 respectively. After iron oxide impregnation, the surface texture shows less spongy structure than CCAC. It is suggested that the formation of well-dispersed iron oxide nanoparticles covering CCAC surface led to such structure.

Transmission electron microscopy: TEM micrograph for the prepared MIONAC as shown in Figure-2. From these micrographs it is observed that the particle size of the nanoparticles lie in the range of 20-80 nm. Fe_3O_4 nanoparticles with a cubic structure are clearly visible in the micrographs. The particles formed tend to cluster as they are magnetic in nature[22]. The primary carbon particles are interconnected with each other to form networks. MIONAC primary particles exhibited a rounded cubic shape with an almost homogenous in size distribution. The iron-oxide nanoparticles are well dispersed.

Table-1: Proximate analysis of raw corn cob, CAC and MIONAC.

Activated Carbon	Moisture %	Ash %	Volatile Matter %	Fixed Carbon %
Corn Cob	6.8	5.8	77	10.4
CCAC	26.7	2.6	22.2	48.5
MIONAC	21.7	15.2	12.4	51.1

Table-2: Ultimate analysis of CCAC and MIONAC.

Activated Carbon	Carbon %	Hydrogen %	Nitrogen %	Sulphur %
Corn Cob	60.93	8.26	5.87	BDL
CCAC	81.40	0.81	1.64	BDL
MIONAC	56.60	0.22	1.44	BDL

BDL: Below detectable limit

Table-3: Characteristics of CCAC and MIONAC

Adsorbent	Iodine number, mg/g	N_2-BETsurface Area, m^2/g	Pore volume, cm^3/g
CCAC	1356	1429	0.7404
MIONAC	702	807	0.3758

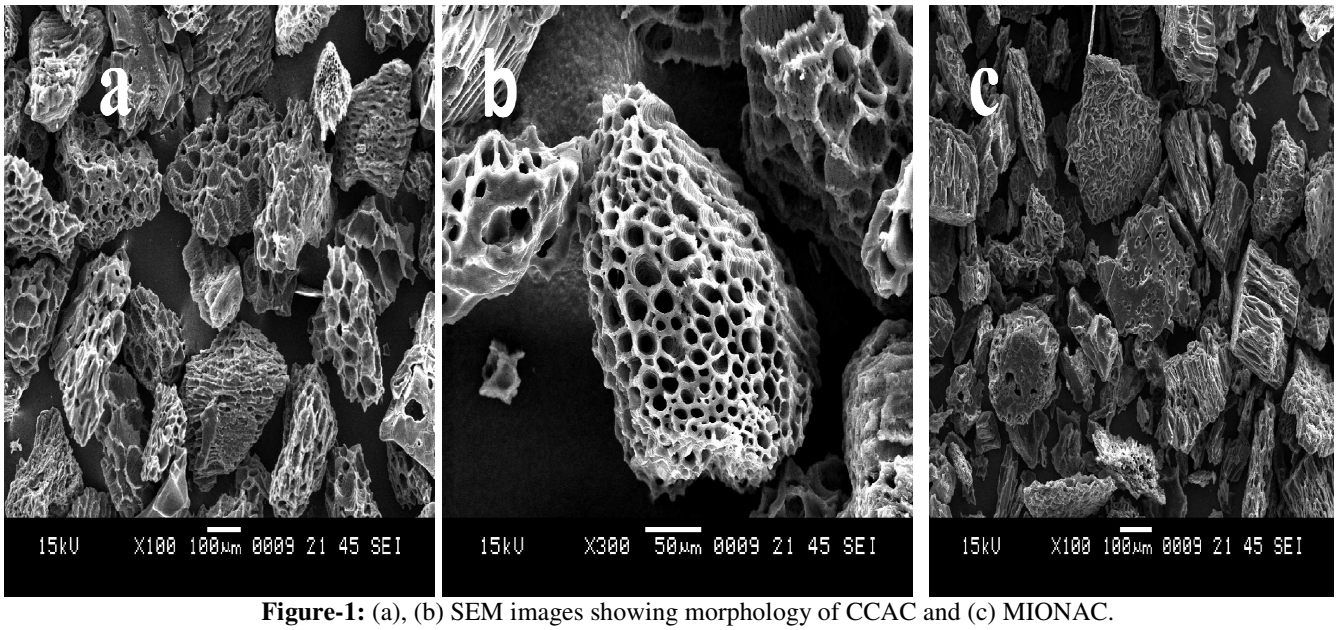

Figure-1: (a), (b) SEM images showing morphology of CCAC and (c) MIONAC.

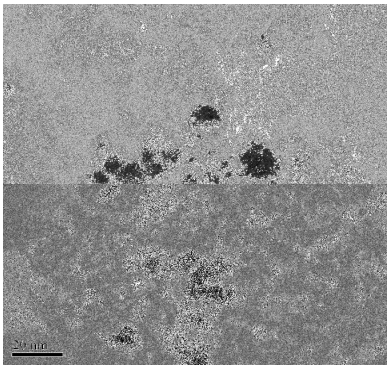

Figure-2: TEM image of MIONAC.

FT-IR spectroscopic analysis: To resolve the functional groups present and its wave numbers, FT-IR of CCAC and MIONAC were carried out by using Fourier transform infrared spectrophotometer (FT-IR) (Perkin Elmer, PE-RXI) in the range of 450-4000cm^{-1}. The FT-IR spectra in Figure-3 (a) and (b) clearly show various surface groups present on the Corncob activated carbon surface and magnetic activated carbon surface. In FT-IR of CCAC (Figure-3 (a)), the predominant presence of free phenolic –OH stretch vibration around 3148 cm^{-1}is observed. The band around 2372cm^{-1} is due to carboxylic O-H stretch vibrations. The band around 1559cm^{-1} is observed due to the presence of carboxylate group COO^-. The peak at 1401cm^{-1} is due to C-N vibrations of aliphatic amine. The spectra around 1000cm$^-$ and below is marked by the noisy spectrum that may due to the presence of mineral matter. In FT-IR spectra of MIONAC (Figure-3 (b)) a broad and strong band at 3747-3272 cm^{-1} is due to the stretching vibrations of –OH, which is assigned to OH^- absorbed by Fe_3O_4 nanopartcles. MIONAC exhibits a carbonyl peak at 1110 cm^{-1}, and peaks at 690 cm^{-1} and 587 cm^{-1} which are attributed to the Fe-O bond vibration of Fe_3O_4 compatible with the presence of iron oxides in the sample[23].

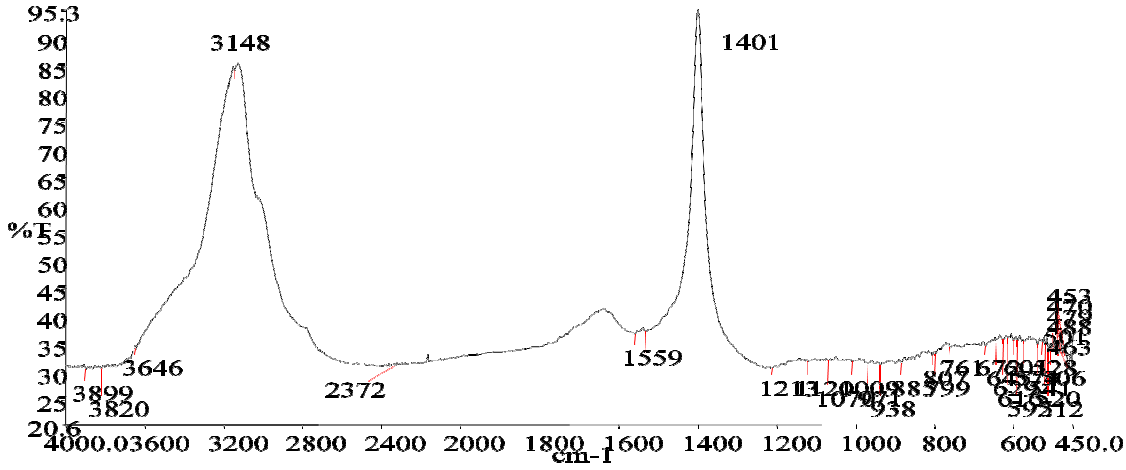

Figure-3: (a) FTIR of CCAC.

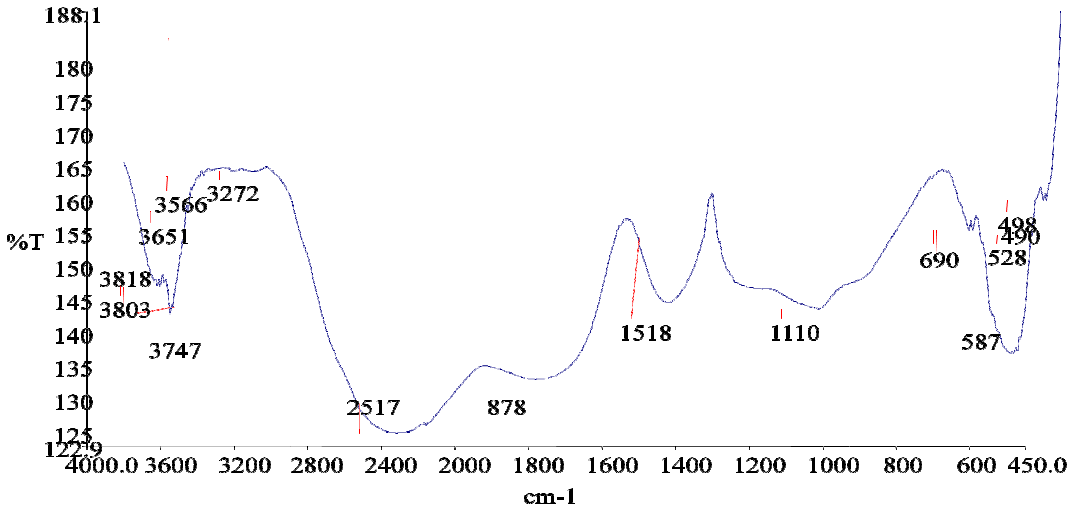

Figure-3: (b) FTIR of MIONAC.

X-ray Diffraction: The X-ray diffraction (XRD) patterns of MIONAC and CCAC were obtained on a powder X-ray diffraction system from analytical model XPERT-PRO diffractometer. Powder XRD are shown in Figure-4 (a) and (b). The XRD of CCAC shows only one broad peak at about $2\theta = 24^0$ which confirms the amorphous nature of the carbon and MIONAC display a sharp peaks at $2\theta = 34.47^0$. The magnetite gives a peak at $2\theta = 34.653^0$ and maghemite gives a peak at $2\theta = 35.597^0$.

Hysteresis and magnetic moment measurements: The magnetic properties of a ferromagnetic material are represented by the plots of magnetization (M) against the field strengths giving the hysteresis loop. The hysteresis measurement was carried out using Lakeshore vibrating sample magnetometer (VSM) 7410 at room temperature. The suitability of ferromagnetic materials for application depends on characteristics shown by their hysteresis loops[24] obtained from plots of magnetization (M) against the field strengths. Magnetization properties were investigated at room temperature by VSM which quantified the magnetic behaviour. The saturation magnetization of magnetic activated carbon is 4.15 emu/g at room temperature as shown in (Figure-5 (a)). However, MIONAC has a good response under the additional permanent magnetization (Figure-5 (b)), which made the solid and liquid phases separate quickly.

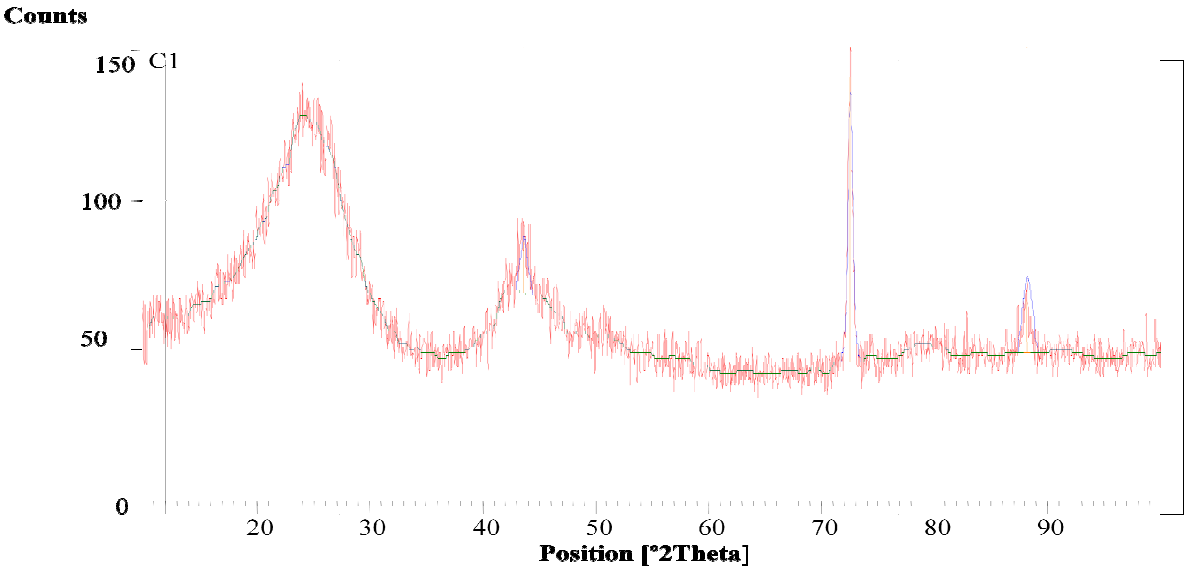

Figure-4: (a) XRD of CCAC.

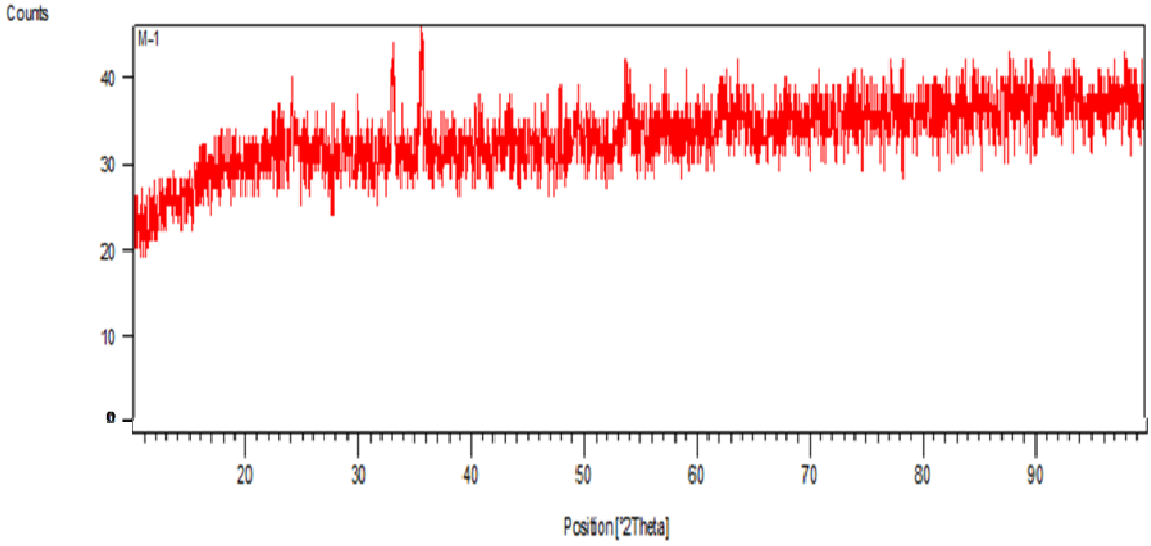

Figure-4: (b) XRD of MIONAC.

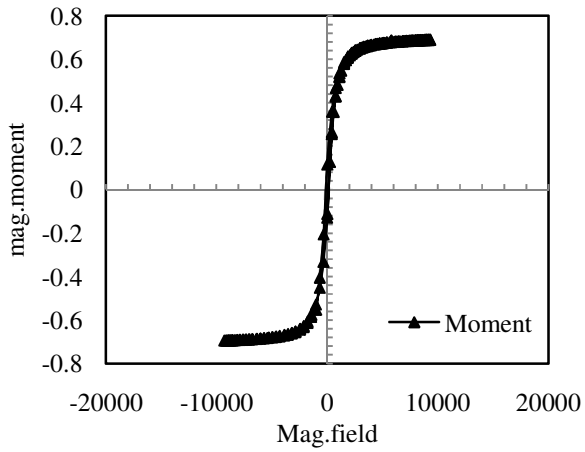

Figure-5: (a) VSM Magnetisation Curve of MIONAC.

Figure-5: (b) MIONAC attracted by magnetic retriever.

Results and discussion

Adsorption isotherms: In order to study the dominant adsorption mechanism and to compute various adsorption parameters three adsorption models, namely Langmuir, Freundlich and BET were used.

Langmuir adsorption model[25] and its parameters strongly indicate the monolayer behaviour of adsorption phase. The linear form of the Langmuir adsorption isotherm is given by the following equation:

$$1/Q_e = (1/Q_0) + (1/Q_0 b) \times 1/C_e$$

Where: Q_e is the amount adsorbed per unit weight of the adsorbent, mg/g at equilibrium, Q_0 is the monolayer capacity of adsorbent, mg/g, C_e is the equilibrium concentration of adsorbate in solution, and b is Langmuir constant.

Langmuir parameters Q_0 and b were calculated from the slope and intercept of the linear plots of $1/Q_e$ vs. $1/C_e$ as depicted in Figure-6(a) and (b) and data are shown in Table-4.

The adsorption data shows that the adsorption capacity (Q_0) value of MIONAC (90mg g-1) is slightly lesser than the CCAC (125 mg g^{-1}) but the separation of adsorbent from the solution is easier by using a magnet. The Q^0 values for phenol adsorption decrease with iron oxide loading. The reduction in Q^0 values can be attributed to reduction in surface area and pore size of iron oxide loaded samples.

The linear form of Freundlich adsorption isotherm[26] is as follows:

$$\log(Q_e) = \log K_f + 1/n \log (C_e)$$

Where: Ce is the equilibrium concentration (mg/L), Qe is the amount adsorbed (mg/g). K_f and n are Freundlich constants related to adsorption capacity and adsorption intensity. The value of K_f and 1/n are obtained from the slope and intercept of the linear Freundlich plot of Log Qe vs. Log Ce in Figure-7(a) and (b) and the values shown in Table-4.

It shows that, the decrease in K_f values reveal a reduction of adsorption capacity of MIONAC due to iron oxide loading. Freundlich constant 1/n is known as indicator of adsorption intensity.

The BET adsorption equation can represented as:

$$C_e/Q_e\,(C_s-C_e) = 1/Q_0 z + (z-1/Q_0 z)*C_e/C_s$$

Where: Q_e is the amount adsorbed per unit weight of the adsorbent, mg/g at equilibrium, Q_0 is the monolayer capacity of adsorbent, mg/g, C_e is the equilibrium concentration of adsorbate in solution, C_s is the saturated concentration of the adsorbate and z is BET constant. BET parameters Q_0 and z were calculated from the graph plotted between C_e/C_s vs $C_e/Q_e\,(C_s-C_e)$ in Figure-8(a) and (b) The values shown in Table-4, it is seen that the Q^0 values decreased for phenol adsorption on MIONAC as compared to CCAC.

Kinetic study for MIONAC: In the present study, a simplified interpretation of the kinetics data based on Langmuir theory[27].

Kinetic study were analysed using Langmuir Kinetic equations,

$$\ln[(C_t-C_e)/(C_t+a)] = -kC_e t + \ln[(C_0-C_e)/(C_0+a)]$$

Where, $a = (C_0/kC_e)$ and $k = Ka/Kd$

Figure-9(a) and (b) shows the adsorption kinetics of phenol onto CCAC and MIONAC and the changes in the phenol concentration with time in aqueous phase. The adsorption rate constant 'Ka' and desorption rate constants 'Kd' thus evaluated by plotting $\ln[(C_t-C_e)/(C_t+a)]$ against t, (Figure-9) and the value of adsorption rate constants for MIONAC are given in Table-4. The Langmuir adsorption kinetics model fits well in the present study as the R^2 value ranges from 0.99.

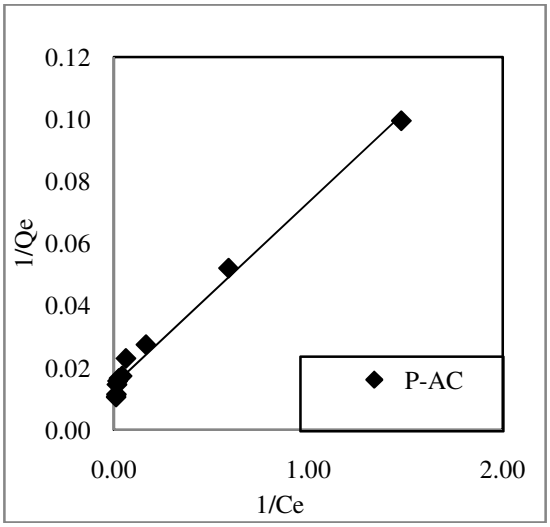

Figure-6a): Langmuir adsorption graph of CCAC.

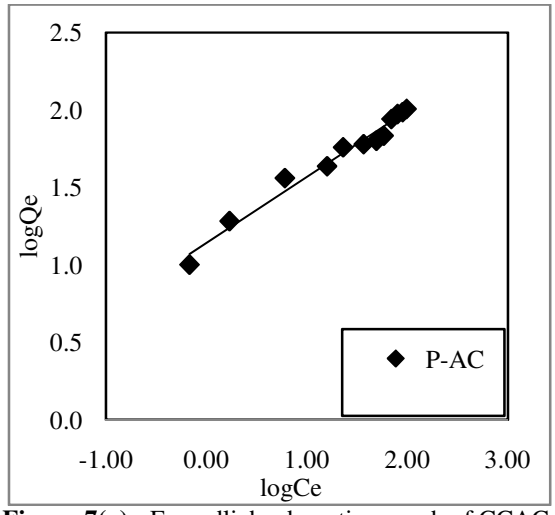

Figure-7(a): Freundlich adsorption graph of CCAC.

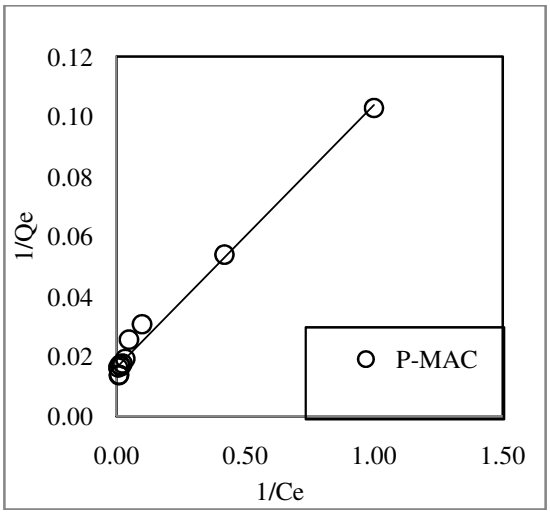

Figure-6b): Langmuir adsorption graph of MIONAC.

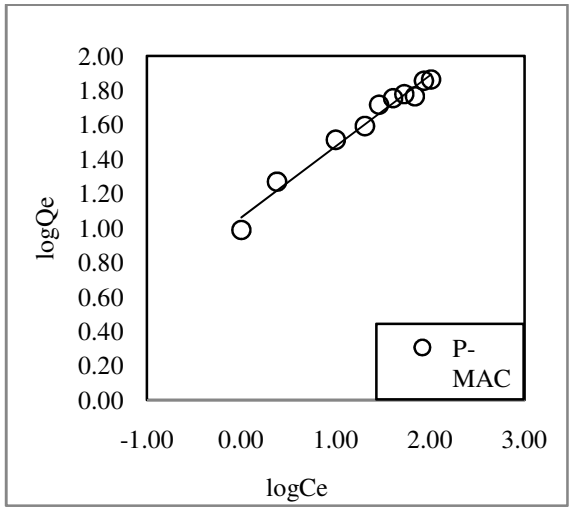

Figure-7(b): Freundlich adsorption graph of MIONAC.

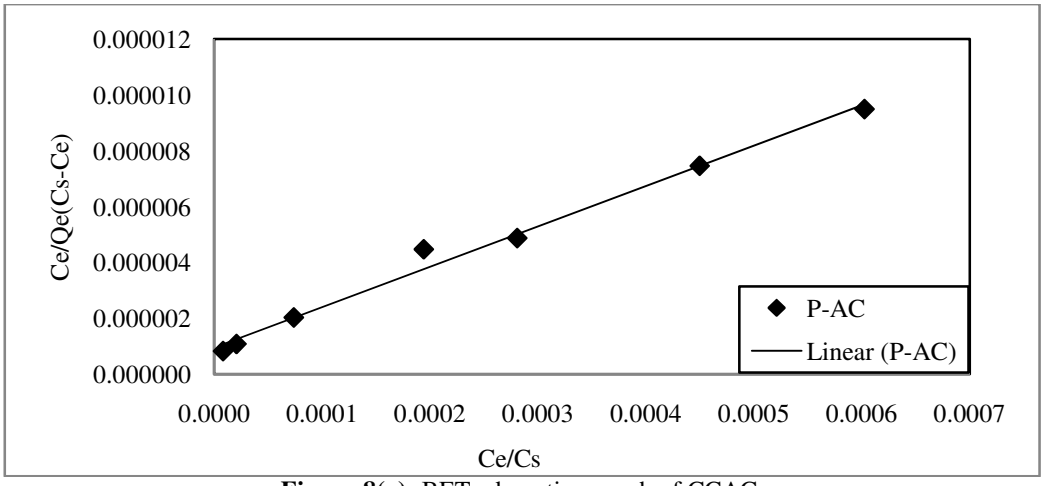

Figure-8(a): BET adsorption graph of CCAC.

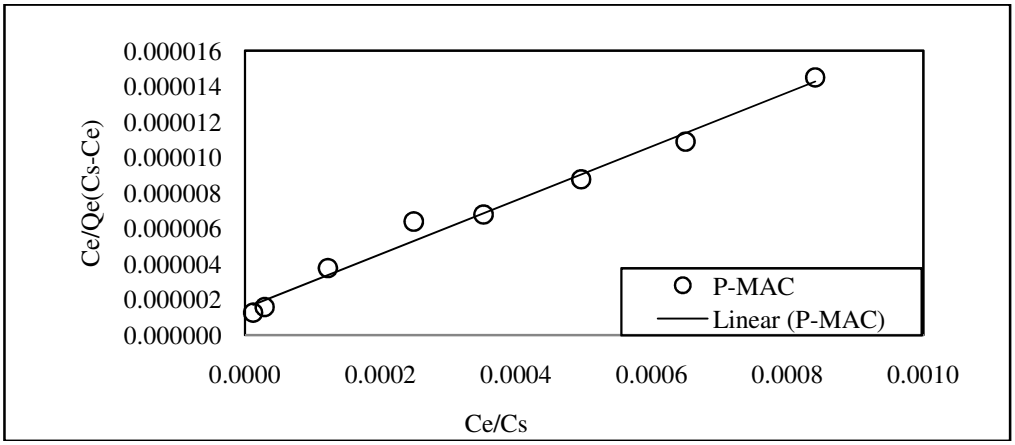

Figure-8(b): BET adsorption graph of MIONAC.

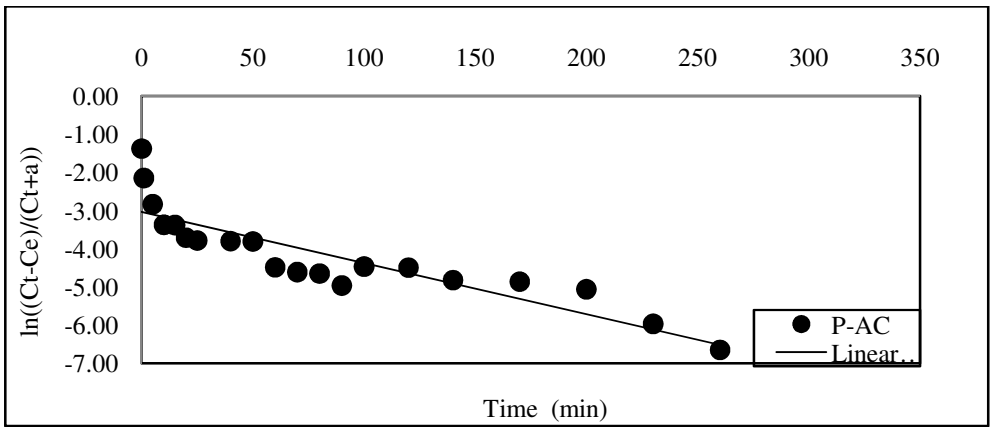

Figure-9(a): Langmuir kinetic graph of CCAC.

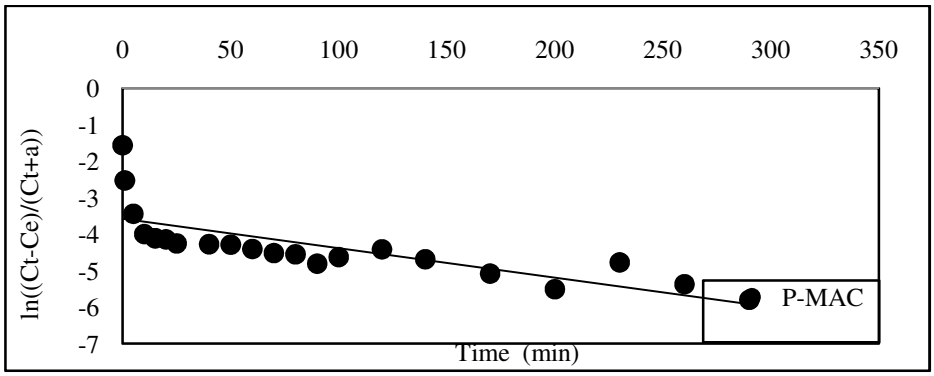

Figure-9(b): Langmuir kinetic graph of MIONAC.

Table-4: Adsorption isotherm constants and kinetic constants for organic pollutants phenol on CCAC and MIONAC.

Sr. No.	Adsorbent	Adsorbate	Langmuir constant		Freundlich constant		BET constant		Kinetics constant	
			Q^0	b	K_f	1/n	Q^0	Z	K_a	K_d
1	CCAC	P	125	0.2105	22.181	0.552	125	6999	19.90	0.0052
2	MIONAC	P	90	0.0378	9.268	0.464	90	3999	9.90	0.0027

Conclusion

Corncob activated carbon (CCAC) and magnetic iron oxide nanoparticles activated carbon (MIONAC) were prepared for the removal of phenol from aqueous waste. The characterisation of corncobs and prepared activated carbon show that the corncobs are potential raw material to prepare activated carbon. SEM of CCAC shows crackes and crevices while SEM of MIONAC shows the dispersion of Fe_3O_4 nanoparticles on activated carbon as the pores are not very clear. FT-IR Spectrum of CCAC and MIONAC show the presence of various surface groups with predominant presence of phenolic –OH. The other surface groups present are carboxylic, carbonyl and aliphatic amines.

The peaks at 690cm^{-1} and 587 cm^{-1} are attributed to Fe-O bond vibration of Fe_3O_4 compatible with the presence of iron oxides in the sample. The XRD of CCAC shows only one broad peak at about $2\theta = 24^0$ which confirms the amorphous nature of the carbon and MIONAC display a sharp peaks at $2\theta = 34.47^0$. The magnetite gives a peak at $2\theta = 34.653^0$ and maghemite gives a peak at $2\theta = 35.597^0$. The TEM of MIONAC shows iron oxide nanoparticles of size 10-20 nm. VSM of MIONAC shows 4.15 emu/g of magnetic strength. The adsorption data shows that the adsorption capacity (Q_0) value of MIONAC (90 mg/g) is slightly lesser than the CCAC (125 mg/g).

Langmuir kinetic model best suits for determination of adsorption and desorption constants for organic pollutants.

References

1. Singh Shripal and Yenkie Mahesh K.N. (2006). Scavenging of Priority Organic Pollutants from Aqueous Waste using Granular Activated Carbon. *Journal of the Chinese Chemical Society*, 53(2), 325-334.

2. Radke C.J. and Prausnitz J.M.J. (1972). Adsorption of organic solutes from dilute aqueous solution of activated carbon. *Ind. Eng. Chem. Fundam*, 11(4), 445-451.

3. Chern J.M. and Chien Y.W.J. (2003). Competitive adsorption of benzoic acid and p-nitrophenol onto activated carbon: isotherm and breakthrough curves. *Water Res*., 37(10), 2347-2356.

4. Fritz W. and Schlünder E.U.J. (1981). Competitive adsorption of two dissolved organics onto activated carbon. *Chemical Engineering Science*, 36(4), 731-741.

5. Srivastava S.K. and Tyagi R.J. (1995). Competitive adsorption of substituted phenols by activated carbon developed from the fertilizer waste slurry. *Wat. Res*., 29(2), 483-488.

6. Khan A.R., Al-Bahri T.A. and Al-Haddad A. (1997). Adsorption of phenol based organic pollutants on activated carbon from multi-component dilute aqueous solutions. *Water Res*., 31(8), 2102-2112.

7. Reinoso Rodriguez F. and Molina-Sabio M. (1992). Activated carbons from lignocellulosic materials by chemical and/or physical activation: an overview *Carbon,* 30(7), 1111-1118.

8. Hu Z. and Vansant E.F. (1995). Carbon molecular sieves produced from walnut shell *Carbon,* 33(5), 561-567.

9. Daud WMA and Ali WSW (2004). Comparison on pore development of activated carbon produced from palm shell and coconut shell *Bioresources Technol.,* (93), 63-69.

10. Gratuito M.K.B., Panyathanmaporn T., Chumnanklang R.A., Sirinuntawittya N. and Dutta A. (2008). Production of activated carbon from coconut shell: optimization using response surface methodology. *Bioresource Technol,* 99(11), 4887-4895.

11. Pondolfo A.G., Amini-Amoli M. and KIllingley J.S. (1994). Activated carbons prepared from shells of different coconut varieties *Carbon,* 32(5), 1015-1019.

12. Caturla F., Molina-Sabio M. and Rodriquez-Reinso F. (1991). Preparation of activated carbon by chemical activation with ZnCl2 *Carbon,* 29(7), 999-1007.

13. Gergova K., Peteov N. and Eser S. (1994). Adsorption properties and microstructure of activated carbons produced from agricultural by- products by steam pyrolysis *Carbon*, 32(4), 693-702.

14. Sentorun-Shalaby C., Ucak-Astarlioglu M.G., Artok L. and Sarici C. (2006). Preparation and characterization of activated carbons by one-step steam pyrolysis/activation from apricot stones.*Microporous and Mesoporous Materials,* 88(1), 126-134.

15. Bouchelta C., Medjram M.S., Bertrand O. and Bellat J.P. (2008). Preparation and characterization of activated carbon from date stones by physical activation with steam. *Applied Pyrolysis,* 82(1), 70-77.

16. Boonamnuayvitaya V., Sae-Ung S. and Tanthapanichakoon W. (2005). Preparation of activated carbons from coffee residue for the adsorption of formaldehyde. *Separation Purification Technol,* 42(2), 159-168.

17. SrinivasaKannan C. and Abu Bakar M.Z. (2004). Production of activated carbon from rubber wood sawdust. *Biomass and Bioenergy*, 27(1), 89-96.

18. Indira T.K. and Lakshmi P.K. (2010). Magnetic Nanoparticles. A review. *Int. J. Pharm. Sci. & Nano technol*., 3(3), 1035-1042

19. Liu Q., Wang L., Xiao A., Gao J., Ding W., Yu H., Huo J. and Ericson Marten (2010). Templated preparation of porous magnetic microspheres and their application in removal of cationic dyes from wastewater. *J. Hazard. Mater*, 181(1), 568-592.

20. Hristov J. and Fachikov L. (2007). An overview of separation by magnetically stabilized beds state of the art and potential applications. *China Particuology,* 5(1), 11-18.

21. Laurent Sophie, Forge Delphine, Port Marc, Roch Alain, Robic Caroline, Elst Luce Vander and Muller Robert N. (2008). Magnetic iron oxide nanoparticles: synthesis, stabilization, vectorization, physicochemical characterization, and biological applications. *Chem. Rev*., 108(6), 2064-2110.

22. Harris P.J.F., Liu Z. and Suenaga K. (2008). Imaging the atomic structure of activated carbon. *Journal of Physics. Condensed Matter*, 20(36), 362201.

23. Marel HWvd and Beutelspacher H. (1976). Atlas of Infrared Spectroscopy of Clay Minerals and their Admixtures. Elsevier: Amsterdam.

24. Jiles D. (2015). Introduction to Magnetism and Magnetic Materials. CRC press.

25. Lanowix IRVING (1918). The adsorption of gases on plane surface of glass, mica and platinum. *J.Am.Chem. Soc*., 30, 1361-1402.

26. Freundlich H.M.F. (1906). Over the adsorption in solution. *Phys. Chem*., 57(385), e470.

27. Todorovic M., Milonjic S.K., Comor J.J. and Gal I.J. (1989). Kinetics of Cs-137 sorption on natural magnetite. Radiation Protection Selected Topics; Dubrovnik Ed. Proceedings of the international radiation protection sysmposium. Yugoslavia, 654-659